Title

Strength analysis of the roller bearing with a crowning and misalignment error

Author(s)

Shuting Li

Journal

Engineering Failure Analysis Volume 123, May 2021, 105311

Published

22 February 2021

URL

https://doi.org/10.1016/j.engfailanal.2021.105311

Strength analysis of the roller bearing with a crowning and misalignment error

Shuting Li*

Department of Mechanical, Electrical and Electronic Engineering, Shimane University, Japan

Abstract

This article aims to present a reliable method that can conduct loading-capacity calculations and strength analyses of roller bearings. A new algorithm and mathematical model are proposed in this paper to realize the purposes through building deformation compatibility relationships and load equilibrium relationships among the outer ring, rollers and the inner ring using mathematical programming method and three-dimensional, finite element method. Special software is developed through many years of efforts to realize the analysis procedures. Contact analysis of a roller bearing is conducted successfully by the developed software. It is found that edge-loads of the roller bearing are analyzed successfully by the developed software when the rollers are not crowned. It is also found that the edge-loads are disappeared and the contact pressure on roller surface becomes a uniform distribution when the rollers are crowned. The effect of quantity of roller-crowning on the contact pressure distribution of rollers is also investigated. It is found that the maximum contact pressure can be reduced about 11% if the quantity of roller-crowning is determined by the maximum roller load. Shear stresses inside the rollers are also analyzed. It is found that the maximum shear stresses exist at the two ends of rollers and near the contact boundaries of the rollers. This means that the roller bearing shall have a fatigue failure at the two ends and near the contact boundaries of the rollers, not at the center of the contact area of the rollers. Finally, contact pressure distribution is analyzed successfully for the roller bearing with a misalignment error.

***Keywords**: Roller Bearing; Crwoning; Misalignment error; Contact pressure; Shear stress.*

1. Introduction

Roller bearings are widely used in various kinds of machines for the sake of the great radial rigidity and high loading-capacity. It is very important to know loading-capacity and radial rigidity of the roller bearings when to use them in machine design. But it is not easy to know them because of the problems of multi-roller contact, roller-crowning, misalignment errors and structural deformation of the bearing. The reality is that it is still an unsolved problem to perform loading-capacity calculation, strength and contact rigidity analyses of the roller bearings in theory.

* Corresponding author at: Department of Mechanical, Electrical and Electronic Engineering, Graduate School of Natural Science and Technology, Shimane University, 1060 Nishikawatsu-Cho, Matsue, 690-8504, Japan
E-mail address: shutingli@ecs.shimane-u.ac.jp

Many studies [1-5] were conducted on bearing contact fatigue failures and it has been understood well that pressure distribution on the contact surfaces and shear stresses inside bearing parts are the main reasons to result in the fatigue failures of the bearing. Also, many studies were conducted on contact analysis and load distribution calculation of bearings. Lovell [6] studied the contact problem of a ball bearing using a model of two disks contacting with a ball numerically. Zhao [7] analyzed roller loads of a roller bearing using a two-dimensional (2D), finite element method (FEM). Kamamoto [8] conducted a study on load carrying capacity of a roller bearing with profile-crowning. Krantz [9] conducted a contact analysis of a roller bearing with the 2D, FEM. Guo [10] also conducted contact analyses of a deep groove ball bearing and a cylindrical roller bearing using three-dimensional (3D), FEM. Tomovic [11] investigated the effect of internal radial clearance on load distribution of a ball bearing theoretically. Wang [12] studied the contact problem of a high-angular contact thrust ball bearing through finite element simulation. Qi [13] also conducted a contact analysis for a deep groove ball bearing in multibody systems theoretically. Nagatani [14] studied the roller load distribution of a roller bearing by suggesting a new theoretical resolution. Bovet [15] predicted the internal behavior of ball bearings under high moment load. Zhang [16] studied the relationship between stiffness and preload for an angular contact ball bearing theoretically. Machado [17] predicted the mechanical behavior of a ball bearing considering rigid and elastic housings using a 2D bearing modeling based on the Discrete Element Method. Li [18] conducted a contact analysis of a roller bearing using the 3D, FEM and one rolling-element model. Though the above-mentioned studies can be available, the problems of multi-roller contact, roller-crowning (edge-load), misalignment error and structural deformation of the roller bearings cannot be solved completely. It is still a problem at the present situation how to calculate surface contact pressure and internal shear stresses of the roller bearings if the multi-roller contact, roller-crowning, misalignment error and structural deformation of the roller bearings are considered.

This article presents a reliable way that can conduct contact analysis and loading-capacity calculation of roller bearings when the multi-roller contact, roller-crowning, misalignment errors and structural deformation of the roller bearings are considered. A numeric method and FEM software are developed to realize this research purpose through many years of research. Edge-loads are analyzed successfully for the roller bearings. It is found that the rate of edge-load is about 26% when the rollers are not crowned. It is also found that the maximum contact pressure on the roller can be reduced about 6% when the rollers are crowned using *Johson-Gohar*'s curve [19]. The effect of the quantity of roller-crowning on contact pressure is also investigated. It is found that the maximum contact pressure on roller surface can be further reduced about 11% if the quantity of roller-crowning is determined by the maximum roller load. Finally, the effect of the misalignment error on contact pressure is investigated when the bearing has 0.05-degree misalignment error.

2. Bearing structure and the roller crowning

Figure 1 is a cylindrical roller bearing (size number NU207E, made by NTN [20]) used as the research object in this paper. There are 14 rollers in the bearing. Diameters of the rollers are 10mm. The basic dynamic load rating is 50.5kN. This bearing is made of SUJ2, a Japanese material name.

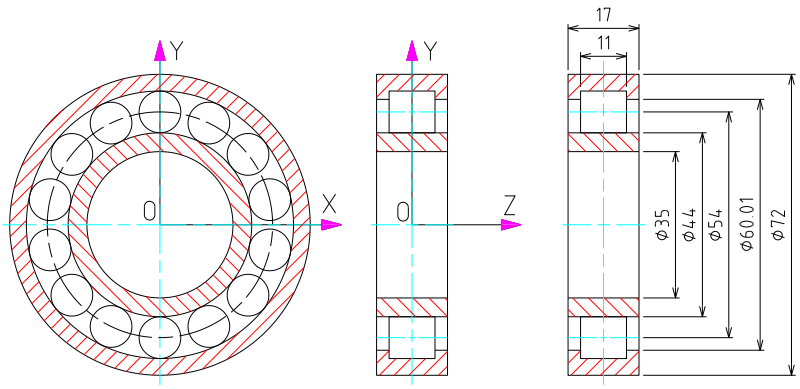

Fig. 1. Structure of the roller bearing (NU207E, NTN)

For the roller bearings, the rollers are usually crowned longitudinally in order to remove edge-loads happened at the two ends of the rollers. Equation (1) was proposed by *Lungdberg* [21] for the purpose of roller-crowning. In Eq. (1), since $q(x)$, the quantity of roller-crowning, shall become infinity at the two ends of the roller ($x = \pm 0.5l$), it is difficult to put Eq. (1) into a practical use. So, Eq. (1) was modified by *Johson-Gohar* [19] through introducing $(1 - 0.3033b/a)$ into Eq. (1). Then Eq. (1) was modified into Eq. (2). Equation (2) is often called *Johson-Gohar's* curve. This curve was actually used for the roller-crowning in bearing design. So, this paper also uses Eq. (2) here for the roller-crowning.

$$q(x) = \frac{2P}{\pi l E'} ln \frac{1}{1 - (2x/l)^2} \tag{1}$$

$$q(x) = \frac{2P}{\pi l E'} ln \frac{1}{1 - (1 - 0.3033b/a)(2x/l)^2} \tag{2}$$

$$\mathrm{E}' = \frac{E}{1 - \nu^2} \tag{3}$$

Where,

$q(x)$: quantity of roller-crowning at the position x.

x : longitudinal position of a point on roller surface. "$x = 0$" stands for the center of the roller. "$x = \pm 0.5l$" stands for the two ends of the roller.

l: effective contact length of the roller, usually equal to the length of the roller.

a: a half of l $(a = l/2)$.

b: a half width of the contact.

E : Young's modulus.

ν : Poisson's ratio.

E′: equivalent Young's modulus calculated by Eq. (3).

P : radial load of the roller bearing

3. Contact analysis of the roller bearing

3.1. Mechanics model of the roller bearing

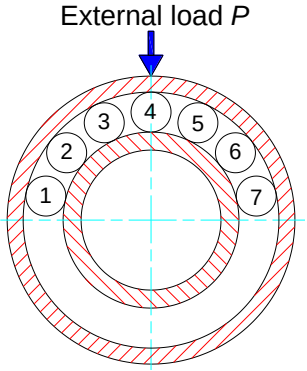

Fig. 2. Mechanics model used for contact analysis of the roller bearing

Figure 2 is a mechanics model used for contact analysis of the roller bearing. Since 14 rollers are used in the bearing. 7 rollers (half of the total number) are used in the model for contact analysis. These 7 rollers are illustrated with the numbers 1, 2, …,7 that stand for the roller positions in the bearing.

Contact analyses of the 7 rollers with the inner and the outer ring are divided into two separate steps. The first step is used to conduct the contact analysis of the 7 rollers with the inner ring and the second step is used to perform the contact analysis of the 7 rollers with the outer ring. These two steps are stated respectively in the following.

3.2. Contact analysis between the inner ring and the 7 rollers

Figure 3 is a sectional view of the 3D, contact model used to perform contact analysis between the inner ring and one roller. In Fig.3, it is assumed that radial load between the roller and the inner ring is denoted as P_i. Also, only elastic deformation is considered in the contact analysis. Contact problem between the inner ring and one roller is solved as shown below.

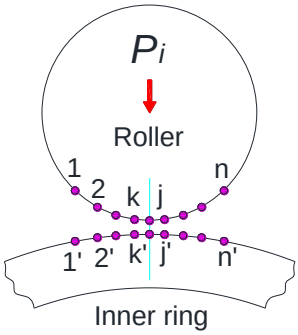

Fig. 3. The contact between the inner ring and one roller

A lot of pairs of contact points, such as (1-1'), (2-2'), …, (k-k'), …, (j-j') and (n-n') in Fig. 3, are made on the contact surfaces of the roller and the inner ring raceway. These pairs are made along the direction of the radial load P_i. This means that the common normal lines of these pairs of contact points are parallel to the direction of P_i. It is assumed that some of the pairs shall contact each other when the load P_i is applied.

For an arbitrary pair (k-k') as shown in Fig. 3, the contact force between the pair (k-k') is denoted as F_k (F_k is along its common normal line), the gap between the pair (k-k') is denoted as ε_k and the radial relative deformation between the inner ring and the roller is denoted as δ_i. The elastic deformation of the pair (k-k') along its common normal line is denoted as ω_k and $\omega_{k'}$ respectively. If the pair (k-k') comes into contact with each other when the load P_i is applied, then ($\omega_k + \omega_{k'} + \varepsilon_k$), the amount of the deformation and the gap of the pair (k-k'), will be equal to δ_i. On the other hand, if the pair (k-k') doesn't come into contact, then ($\omega_k + \omega_{k'} + \varepsilon_k$) will be greater than δ_i. These relationships are deformation compatibility relationships of the pair (k-k') and can be expressed with Eq. (4) and Eq. (5) individually. Also, they can be summarized into Eq. (6).

$$\omega_k + \omega_{k'} + \varepsilon_k - \delta_i = 0 \quad \text{(Contact)} \tag{4}$$

$$\omega_k + \omega_{k'} + \varepsilon_k - \delta_i > 0 \quad \text{(Not contact)} \tag{5}$$

$$\omega_k + \omega_{k'} + \varepsilon_k - \delta_i \geq 0 \quad (k = 1, 2, \dots, n) \tag{6}$$

Since the pair (k-k') is an arbitrary pair, Eq. (6) can be suitable for all the pairs made on the contact surfaces. So, k can be varied from 1 to n. Here, n is the total number of the pairs of contact points made on the contact surfaces.

On the other hand, since the elastic deformation ω_k and $\omega_{k'}$ can be expressed using deformation influence coefficients and contact forces of the contact points, Eq. (7) and Eq. (8) can be obtained.

$$\omega_k = \sum_{j=1}^{n} a_{kj} F_j \tag{7}$$

$$\omega_{k'} = \sum_{j=1}^{n} a_{k'j'} F_j \tag{8}$$

Where, a_{kj} and $a_{k'j'}$ are the deformation influence coefficients of the contact points along their common normal lines. a_{kj} and $a_{k'j'}$ can be calculated using 3D, FEM. F_j is the contact force between the pair (j-j') of contact points.

If Eq. (7) and Eq. (8) are substituted into Eq. (6), then Eq. (9) can be available. If Eq. (9) is written into a form of matrix expression, then Eq. (10) can be available.

$$\sum_{j=1}^{n} \left[a_{kj} + a_{k'j'} \right] \times F_j + \varepsilon_k - \delta_i \geq 0 \tag{9}$$

$$[S]\{F\} + \{\varepsilon\} - \delta_i\{e\} \geq \{0\} \tag{10}$$

Where,

$[S] = [S_{kj}] = [a_{kj} + a_{k'j'}]$

$\{F\} = \{F_1,\ F_2,\ \dots,\ F_j, \dots, F_n\}^T$

$\{\varepsilon\} = \{\varepsilon_1,\ \varepsilon_2,\ \dots,\ \varepsilon_k, \dots, \varepsilon_n\}^T$

$(k = 1,\ 2,\ 3, \dots, n;\ \ j = 1,\ 2,\ 3,\ \dots,\ n)$

$\{e\} = \{1,\ 1, \dots, 1\}^T$

$\{0\} = \{0,\ 0, \ldots, 0\}^T$

Except for the deformation compatibility relationship, a load equilibrium relationship as given in Eq. (11) can be available for the pairs of contact points.

$$\sum_{k=1}^{n} F_k = P_{\mathrm{i}} \qquad (k = 1, 2, \ldots, n) \qquad (11)$$

If Eq. (11) is written into a form of matrix expression, then Eq. (12) can be available.

$$\{e\}^T\{F\} = P_{\mathrm{i}} \qquad (12)$$

In the case of the multi-roller contact, for an example, in the case of this paper, there are 7 rollers in contact with the inner ring and the outer ring when the bearing is loaded. So, a contact model of 7 rollers is made as shown in Fig. 4. Contact analysis of this model can be conducted as follows.

Figure 4 is a sectional view of the 3D, mechanics model used for contact analysis between the inner ring and the 7 rollers. Radial loads on the 7 rollers are denoted as P_1, P_2, P_3, P_4, P_5, P_6 and P_7 respectively when the total external load P is applied on the bearing vertically as shown in Fig. 2. In order to understand the contact analysis procedures easily, it is assumed that the 7 centers of the 7 rollers are fixed on the distribution circle (usually, called "pitch circle" of the rollers). Also, it can be assumed that the pitch circle is a rigid circle without deformation. The total vertical deformation of the inner ring relative to the pitch circle is denoted as δ_{01} when the external load P is applied. Radial deformation of every roller relative to the inner ring is denoted as δ_1, δ_2, δ_3, δ_4, δ_5, δ_6 and δ_7 respectively.

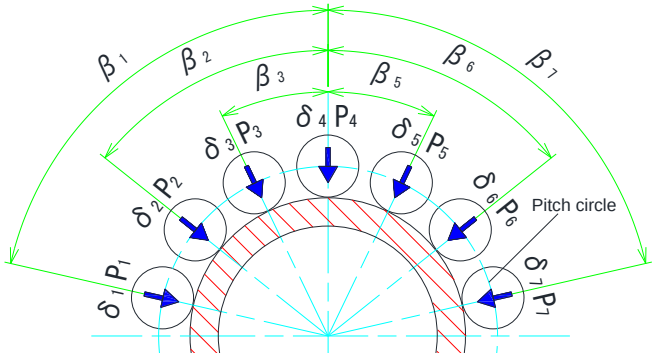

Fig. 4. Contact between the inner ring and 7 rollers

Since a relationship exists between the total deformation of the bearing and the local deformation of every roller, Eq. (13) can be available. Where, β_1, β_2, β_3, β_4, β_5, β_6 and β_7 are position angles of the rollers as shown in Fig. 4. $\beta_4 = 0°$ for the roller No. 4.

$$\begin{cases} \delta_1 = \delta_{01} \times \cos\beta_1 & (\text{Roller } 1) \\ \delta_2 = \delta_{01} \times \cos\beta_2 & (\text{Roller } 2) \\ \delta_3 = \delta_{01} \times \cos\beta_3 & (\text{Roller } 3) \\ \delta_4 = \delta_{01} \times \cos\beta_4 & (\text{Roller } 4) \\ \delta_5 = \delta_{01} \times \cos\beta_5 & (\text{Roller } 5) \\ \delta_6 = \delta_{01} \times \cos\beta_6 & (\text{Roller } 6) \\ \delta_7 = \delta_{01} \times \cos\beta_7 & (\text{Roller } 7) \end{cases} \quad (13)$$

Also, since the deformation compatibility relationship in Eq. (10) is made for an arbitrary roller, this relationship can also be suitable for all the rollers used in the contact analysis. So, in the case of 7 rollers, the following deformation compatibility relationships as shown in Eq. (14) can be available.

$$\begin{cases} [S]_1\{F\}_1 + \{\varepsilon\}_1 - \delta_1\{e\}_1 \geq \{0\}_1 & (\text{Roller } 1) \\ [S]_2\{F\}_2 + \{\varepsilon\}_2 - \delta_2\{e\}_2 \geq \{0\}_2 & (\text{Roller } 2) \\ [S]_3\{F\}_3 + \{\varepsilon\}_3 - \delta_3\{e\}_3 \geq \{0\}_3 & (\text{Roller } 3) \\ [S]_4\{F\}_4 + \{\varepsilon\}_4 - \delta_4\{e\}_4 \geq \{0\}_4 & (\text{Roller } 4) \\ [S]_5\{F\}_5 + \{\varepsilon\}_5 - \delta_5\{e\}_5 \geq \{0\}_5 & (\text{Roller } 5) \\ [S]_6\{F\}_6 + \{\varepsilon\}_6 - \delta_6\{e\}_6 \geq \{0\}_6 & (\text{Roller } 6) \\ [S]_7\{F\}_7 + \{\varepsilon\}_7 - \delta_7\{e\}_7 \geq \{0\}_7 & (\text{Roller } 7) \end{cases} \quad (14)$$

If Eq. (13) is substituted into Eq. (14) and Eq. (14) is summarized together, then Eq. (15) can be obtained.

$$[A]\{F\} + \{\varepsilon\} - \delta_{01}\{e'\} \geq \{0\} \quad (15)$$

Where,

$$[A] = \begin{bmatrix} [S]_1 & [0] & \cdots & [0] & [0] \\ [0] & [S]_2 & & [0] & [0] \\ \vdots & & \ddots & \vdots & \\ [0] & [0] & & [S]_6 & [0] \\ [0] & [0] & \cdots & [0] & [S]_7 \end{bmatrix} \quad (7n \times 7n)$$

$$[0] = \begin{bmatrix} 0 & \cdots & 0 \\ \vdots & \ddots & \vdots \\ 0 & \cdots & 0 \end{bmatrix} \quad (\mathrm{n} \times \mathrm{n})$$

$$\{F\} = \begin{Bmatrix} \{F\}_1 \\ \{F\}_2 \\ \vdots \\ \{F\}_6 \\ \{F\}_7 \end{Bmatrix} \quad (7\mathrm{n} \times 1)$$

$$\{\varepsilon\} = \begin{Bmatrix} \{\varepsilon\}_1 \\ \{\varepsilon\}_2 \\ \vdots \\ \{\varepsilon\}_6 \\ \{\varepsilon\}_7 \end{Bmatrix} \quad (7\mathrm{n} \times 1)$$

$$\{e'\} = \begin{Bmatrix} \{e\}_1 \cos\beta_1 \\ \{e\}_2 \cos\beta_2 \\ \vdots \\ \{e\}_6 \cos\beta_6 \\ \{e\}_7 \cos\beta_7 \end{Bmatrix} = \begin{Bmatrix} \begin{Bmatrix} \cos\beta_1 \\ \cos\beta_1 \\ \vdots \\ \cos\beta_1 \end{Bmatrix} \\ \begin{Bmatrix} \cos\beta_2 \\ \cos\beta_2 \\ \vdots \\ \cos\beta_2 \end{Bmatrix} \\ \vdots \\ \begin{Bmatrix} \cos\beta_6 \\ \cos\beta_6 \\ \vdots \\ \cos\beta_6 \end{Bmatrix} \\ \begin{Bmatrix} \cos\beta_7 \\ \cos\beta_7 \\ \vdots \\ \cos\beta_7 \end{Bmatrix} \end{Bmatrix} \qquad (7n \times 1)$$

$$\{0\} = \begin{Bmatrix} \{0\}_1 \\ \{0\}_2 \\ \vdots \\ \{0\}_6 \\ \{0\}_7 \end{Bmatrix} \qquad (7\mathrm{n} \times 1)$$

In the same way, the load equilibrium relationship in Eq. (12) can also be suitable for all the 7 rollers. Then Eq. (16) can be available.

$$\begin{cases} \{e\}_1^T\{F\}_1 = P_1 & (\text{Roller } 1) \\ \{e\}_2^T\{F\}_2 = P_2 & (\text{Roller } 2) \\ \{e\}_3^T\{F\}_3 = P_3 & (\text{Roller } 3) \\ \{e\}_4^T\{F\}_4 = P_4 & (\text{Roller } 4) \\ \{e\}_5^T\{F\}_5 = P_5 & (\text{Roller } 5) \\ \{e\}_6^T\{F\}_6 = P_6 & (\text{Roller } 6) \\ \{e\}_7^T\{F\}_7 = P_7 & (\text{Roller } 7) \end{cases} \qquad (16)$$

On the other hand, since there is a load equilibrium relationship between the total load P and the local load P_{i} (i=1, 2, .., 7) on every roller, Eq. (17) can be available. If Eq. (16) is substituted into Eq. (17) and Eq. (17) is written into a matrix expression, then Eq. (18) can be available.

$$P_1\cos\beta_1 + P_2\cos\beta_2 + P_3\cos\beta_3 + P_4\cos\beta_4 + P_5\cos\beta_5 + P_6\cos\beta_6 + P_7\cos\beta_7 = P \qquad (17)$$

$$\{e'\}^T\{F\} = P \qquad (18)$$

A mathematical model is made as follows to solve Eq. (15) and Eq. (18) using the mathematical programming method. Since Eq. (15) is an inequality equation that may be strictly positive or identically zero, it can be transformed into an equality equation if so-called slack variables $\{Y\} = \{Y_1, Y_2, \dots, Y_k, \dots, Y_{7n}\}^T$ are introduced in Eq. (15) and let

$[A]\{F\} + \{\varepsilon\} - \delta_{01}\{e'\} = [I]\{Y\}$. Then Eq. (19) and Eq. (20) can be obtained. Where, $[I]$ is a unit matrix of $7n \times 7n$.

$$[A]\{F\} + \{\varepsilon\} - \delta_{01}\{e'\} - [I]\{Y\} = \{0\} \quad (19)$$

$$-[A]\{F\} + \delta_{01}\{e'\} + [I]\{Y\} = \{\varepsilon\} \quad (20)$$

Now, two equality equations of Eq. (18) and (20) are available. They can be used as constrain conditions in the mathematical programming method. In order to solve Eq. (18) and Eq. (20), it is necessary to make an objective function Z. According to the principle of the mathematical programming method, the objective function Z can be made artificially through introducing so-called artificial variables (some positive variables) X_{7n+1}, X_{7n+2}, ..., X_{7n+7n}, $X_{7n+7n+1}$. Finally, the mathematical model for the contact analysis of the inner ring with the 7 rollers is made as follows.

Mathematical model for contact analysis of the inner ring with the 7 rollers

Objective Function:

$$Z = X_{7n+1} + X_{7n+2} + \cdots + X_{7n+7n} + X_{7n+7n+1} \quad (21)$$

Constraint Conditions:

$$-[A]\{F\} + \delta_{01}\{e'\} + [I]\{Y\} + [I]\{Z'\} = \{\varepsilon\} \quad (22)$$

$$\{e'\}^T\{F\} + X_{7n+7n+1} = P \quad (23)$$

Where,

$\{Z'\} = \{X_{7n+1}, X_{7n+2}, \dots, X_{7n+7n}\}^T$

$\{Y\} = \{Y_1, Y_2, \dots, Y_k, \dots, Y_{7n}\}^T$

$Y_k \geq 0 \ \ (k = 1, 2, \dots, 7n)$

$X_{7n+m} \geq 0 \ \ (m = 1, 2, \dots, 7n + 1)$

3.3. Contact analysis between the outer ring and the 7 rollers

Figure 5 is a sectional view of the 3D, contact model used for the contact analysis between the outer ring and one roller. Figure 6 is a sectional view of the 3D, contact model used for the contact analysis between the outer ring and the 7 rollers. In the case of the outer ring contact, a mathematical model used for the contact analysis of the outer ring can be made in the same way as the inner ring. This model is omitted here.

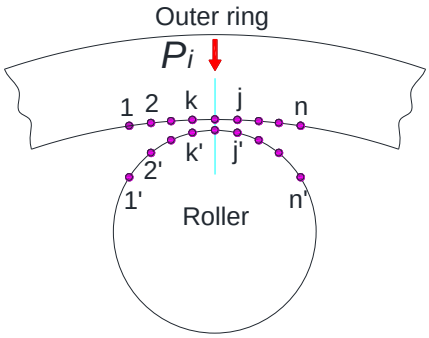

Fig. 5. Contact between the outer ring and one roller

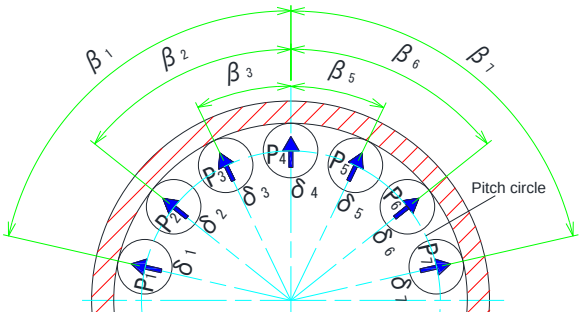

Fig. 6. Contact between the outer ring and the 7 rollers

3.4. Software development

Special software is developed to realize the procedures of the two steps of bearing contact analyses. In the software development, 3D, FEM is used to calculate the deformation influence coefficients a_{kj}, $a_{k'j'}$ that are necessary to make the matrix $[A]$ in Eq. (22). Contact loads between the pairs of contact points can be available after the equations in the mathematical model are solved. Contact pressure between the pairs of contact points is calculated through calculating the contact load distributed on a unit contact area. Internal stresses of the rollers are analysed by 3D, FEM when the contact loads on roller surfaces are available. Calculation results are stated in the following.

4. Calculation results and discussions

Loaded bearing contact analysis is contacted for the roller bearing as shown in Fig. 1 using the developed FEM software. Mesh-dividing patterns of the bearing and roller are given in Fig.7. In order to divide FEM meshes of the roller easily, a small hollow hole is made in the center along the roller axis as shown in Fig. 7 and Fig. 8. The hollow hole surface of the roller, the inside surface of the inner ring and the outside surface of the outer ring are fixed as FEM boundary conditions when to calculate the deformation influence coefficients a_{kj}, $a_{k'j'}$.

In Fig. 8, a local coordinate system $(o_2 - x_2y_2z_2)$ is made for the roller. The coordinate plane $(o_2 - z_2y_2)$ as shown in Fig. 8(a) is called Section 1 and the coordinate plane $(o_2 - x_2y_2)$ as shown in Fig. 8(b) is called Section 2 in this paper. Internal stresses distributed on Section 1 and Section 2 shall be introduced later.

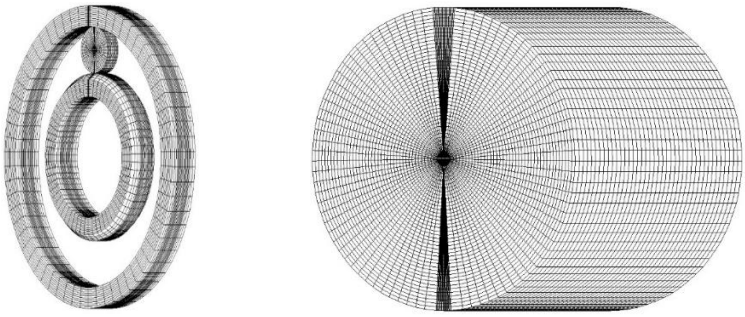

(a) Roller bearing (b) Roller

Fig. 7. Mesh-dividing patterns of the roller bearing and the roller

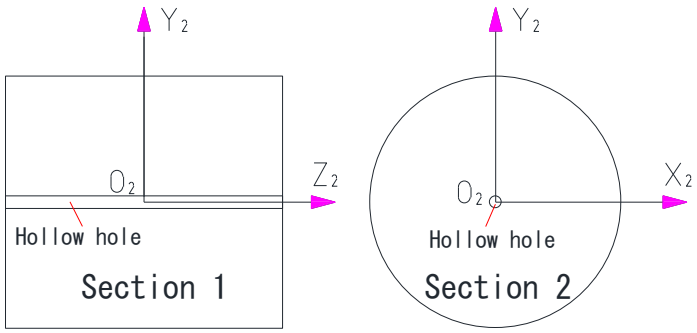

(a) Section 1 (b) Section 2

Fig. 8. The coordinate system $(o_2 - x_2y_2z_2)$ made for the roller

Figure 9 is used to explain the calculation results given in Figs. 10, 11, 13 and 16. As shown in Fig. 9, the roller is placed vertically. This means that the roller axis is vertical. Length of the roller is illustrated with "Roller Length". On the roller surface in Fig. 9(a), there is a hatched area. This hatched area is used for the bearing contact analysis. The length of the hatched area is the roller length and the width of this area is illustrated with "Contact width of the roller". Figure 9(b) is an enlarged view of the hatched area. Figures 10, 11, 13 and 16 are the calculated contact pressure distributed on this hatched area as shown in Fig. 9(b).

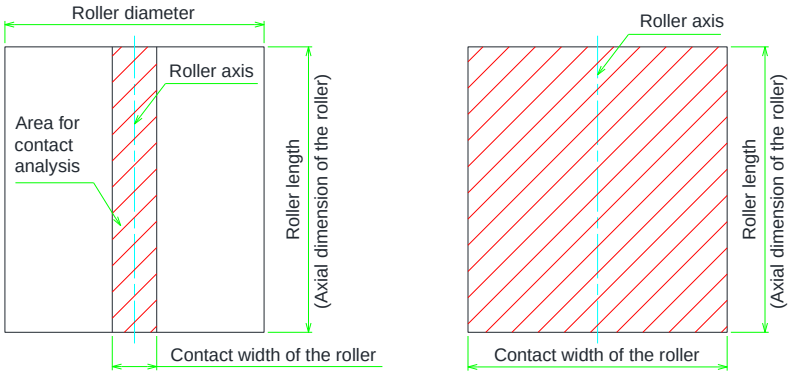

(a) A roller surface (b) Area for contact analysis

Fig. 9. A hatched area on roller surface used for contact analysis

4.1. Contact analysis of the roller bearing without crowning

Contact analysis is conducted firstly for the roller bearing without roller-crowning using the developed software under the external load P=50.5kN, the basic dynamic load rating of the bearing. Calculation results are given in the following.

Figures 10(a)-(d) are calculated contact pressure distributions on the lower surfaces of the rollers No. 4, 3, 2 and 1 respectively. In Fig. 10, the abscissa is the contact width of the roller as shown in Fig. 9(b) and the ordinate is the axial dimension of the roller as shown in Fig. 9(b). From Fig. 10, it is found that the contact pressure distributions take the shapes of rectangles and there are two edge-load areas existing at the two ends of the rollers (the upper and lower ends in Fig. 10). This is because the longitudinal shape of the rollers is a straight line without crowning. So, the straight line profile results in the edge-loads happened at the two ends of the rollers.

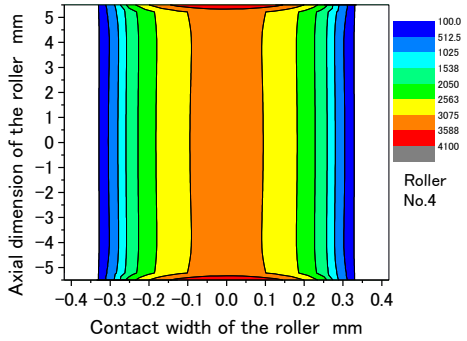

(a) Pressure distribution on the roller 4

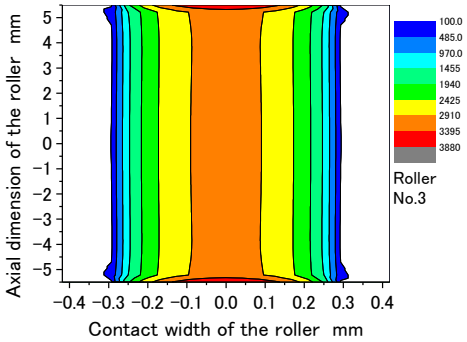

(b) Pressure distribution on the roller 3

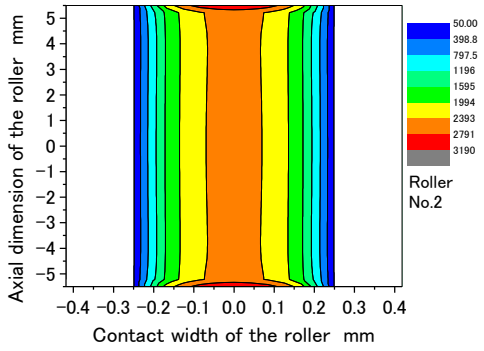

(c) Pressure distribution on the roller 2

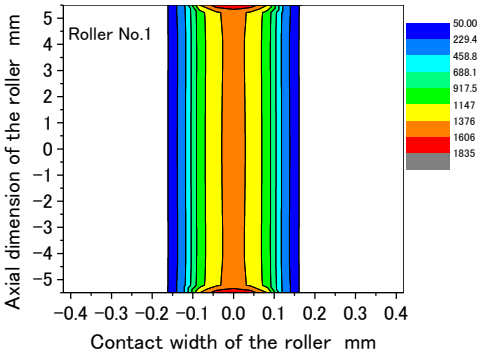

(d) Pressure distribution on the roller 1

Fig. 10. Contact pressure distributed on the roller surface (MPa) (without crowning)

In Fig. 10, the maximum contact pressure at the middle of the roller is denoted as P_M and the maximum contact pressure at the edge-load areas is denoted as P_E. P_M and P_E can be figured out from Fig. 10. Rate of the edge-load is calculated through $(P_E - P_M)/P_M$ and given in Tab. 1. From Tab.1, it is found that all the rollers almost have the same rate of the edge-load (about 26%). It is also found in Tab. 1 that the maximum contact pressure becomes greater when the roller position is closer to the center, the position of the roller 4 in Fig.2. Since contact pressure distributions on the rollers 5, 6 and 7 are calculated to be the same values as the rollers 3, 2 and 1 respectively, they are omitted here.

Tab.1 Rate of the edge-load of the rollers without crowning

Roller Number	P_M (MPa)	P_E (MPa)	$(P_E - P_M)$ (MPa)	$\frac{P_E - P_M}{P_M} \times 100\%$
No. 1	1437	1831	394	27.4%
No. 2	2526	3180	654	25.9%
No. 3	3076	3872	796	25.9%
No. 4	3244	4087	843	26.0%

4.2. Contact analysis of the roller bearing with usual crowning

Contact analysis is conducted for the roller bearing with usual crowning using the developed software under the external load P=50.5kN. The rollers are crowned using *Johson-Gohar's* curve and the quantity of crowning is determined under the basic dynamic load rating 50.5kN. The other conditions are the same as Section 4.1. Calculation results are given in the following.

Contact pressure distributions on the lower surfaces of the roller 4, 3, 2 and 1 are given in Figs. 11 (a), (b), (c) and (d) respectively. From Fig. 11, it is found that the contact pressure distributions are changed from a rectangular shape into an elliptical shape. Also, the edge-load areas disappeared because of the longitudinal crowning of the rollers.

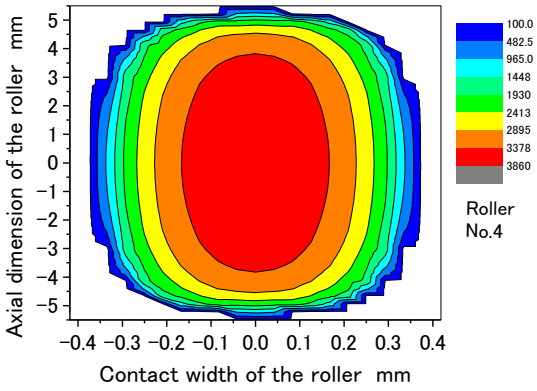

(a) Pressure distribution on the roller 4

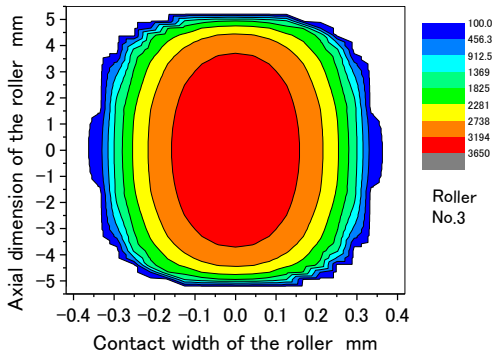

(b) Pressure distribution on the roller 3

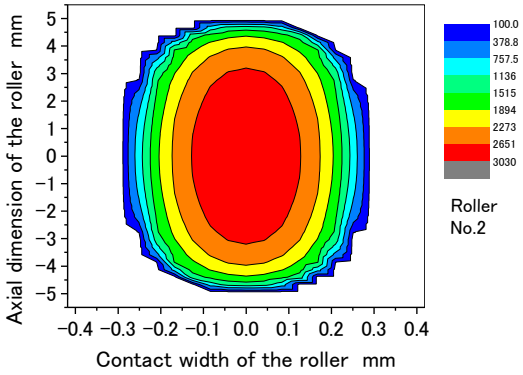

(c) Pressure distribution on the roller 2

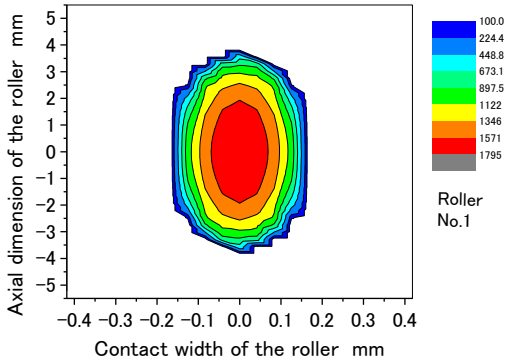

(d) Pressure distribution on the roller 1

Fig. 11. Contact pressure distributed on the roller surface (MPa) (usual crowning)

The maximum contact pressure values on the roller 1, 2, 3 and 4 are figured out from Fig. 11 and denoted as P_c. P_c and P_E (figured out from Fig. 10) are compared in Tab. 2. From Tab. 2, it is found that the maximum contact pressure values on all the rollers are reduced because of the longitudinal crowning of rollers. Reduction rate of the maximum contact pressure is calculated through $(P_E - P_C)/P_C$ and given in Tab. 2. From Tab. 2, it is found that the maximum contact pressure on the roller 4 is reduced about 5.9%. Table 2 also indicates that it is absolutely necessary to make a crowning for the rollers in order to remove edge-loads and extend bearing life.

Tab.2 The maximum contact pressure and reduction rate of the pressure

Roller Number	P_C (MPa)	P_E (MPa)	$(P_C - P_E)$ (MPa)	$\frac{P_C - P_E}{P_C} \times 100\%$
No. 1	1793	1831	-38	-2.1%
No. 2	3024	3180	-156	-4.9%
No. 3	3649	3872	-223	-5.8%
No. 4	3844	4087	-243	-5.9%

Loads and load-sharing ratios of the rollers are also calculated under 50.5kN and illustrated in Fig.12 simultaneously. In Fig. 12, the abscissa is the roller number given in Fig. 2 and the ordinates on the left side and on the right side are the roller load and the load-sharing ratio respectively. From Fig. 12, it is found that the roller 1 and the roller 7, the roller 2 and the roller 6, also the roller 3 and the roller 5 are the same levels of the load and load-sharing ratio. This symmetrical phenomenon is very reasonable in theory. It is also found that the roller 4 has the maximum load 11715N and shares about 23% of the total radial load *P*.

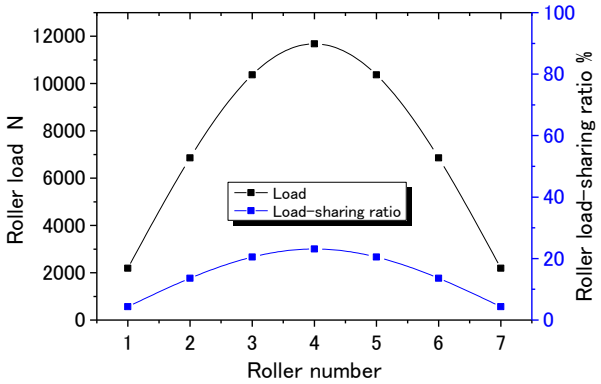

Fig. 12. Load and load-sharing ratio of the rollers

4.3. Contact analysis of the roller bearing with best crowning

Usually, it is difficult to know the roller loads and load-sharing ratios in advance when to design a roller bearing. If the roller loads can be analyzed in theory before the roller bearing is designed, the roller loads can be used to determine the quantity of crowning. For an example in this paper, it is found that the roller 4 has the maximum load of 11715N in Fig. 12. This load is used to determine the quantity of crowning using *Johson-Gohar's* curve at the first and then the loaded bearing contact analysis is conducted for the roller bearing under this quantity of crowning and the same conditions as Section 4.2. In order to distinguish this crowning with the crowning used in Section 4.2, this crowning is called "best crowning" here. Calculation results under the best crowning are given in the following.

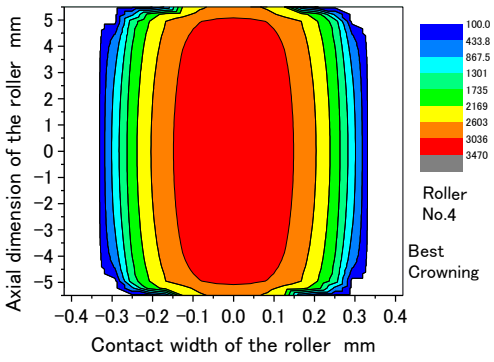

(a) Pressure distribution on the roller 4

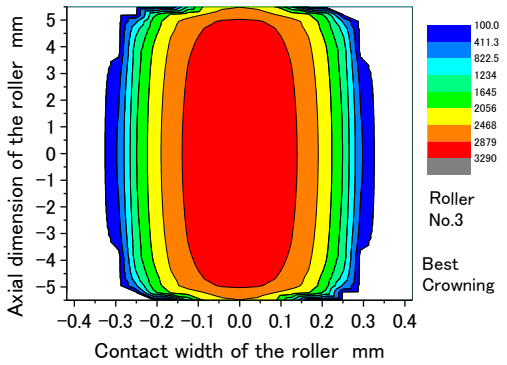

(b) Pressure distribution on the roller 3

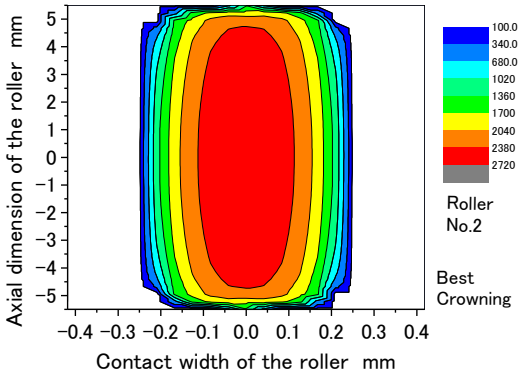

(c) Pressure distribution on the roller 2

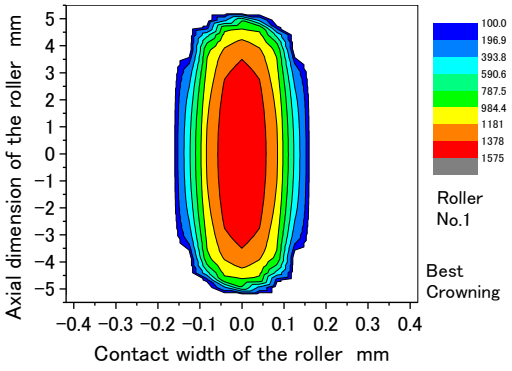

(d) Pressure distribution on the roller 1

Fig. 13. Contact pressure distributed on the roller surface (MPa) (best crowning)

Contact pressure distributions on the lower surfaces of the roller 4, 3, 2 and 1 are given in Figs. 13 (a), (b), (c) and (d) respectively. From Fig. 13, it is found that the contact areas become even larger and the contact pressure distributions become more uniform than Fig. 12 if the best crowning is made.

The maximum contact pressure values on the roller 1, 2, 3, 4 are figured out and denoted as P_{BC}. P_{BC} are compared with P_C in Tab. 3. From Tab. 3, it is found that the maximum pressure values P_{BC} are further decreased by the best crowning. Reduction rate of the maximum pressure is calculated through $(P_{BC} - P_C)/P_{BC}$ and given in Tab. 3. It is found that the maximum contact pressure on the roller 4 is reduced about 11%. This is a great reduction in the contact pressure. It means that the bearing life can be considerably extended if the best crowning is used for the roller bearing in a practical bearing design.

Tab.3 Reduction rate of the contact pressure under the best crowning

Roller Number	P_{BC} (MPa)	P_C (MPa)	$(P_{BC} - P_C)$ (MPa)	$\frac{P_{BC} - P_C}{P_{BC}} \times 100\%$
No. 1	1572	1793	-221	-14%
No. 2	2718	3024	-306	-11%
No. 3	3285	3649	-364	-11%
No. 4	3469	3844	-375	-11%

4.4. Contact analysis of the roller bearing with a misalignment error

Usually, misalignment errors between housing holes and shafts are existing in machines. So, it is necessary to know the effect of the misalignment error on loading-capacity of the bearings. Figure 14 is an image of the roller bearing parts contacted with each other under a misalignment error. As shown in Fig. 14, the outer ring and the roller are inclined by the misalignment error. So, there shall be an angle θ existing between the rollers and the inner ring. This angle is often called tilting angle of the roller. Though it is quite difficult to conduct the loading-capacity calculation of the roller bearings with a misalignment error, the methods presented in this paper can do this calculation well. Figure 15 is the model used for contact analysis between the inclined roller and the inner ring.

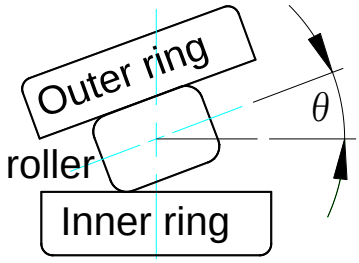

Fig. 14. Bearing contact under a misalignment error

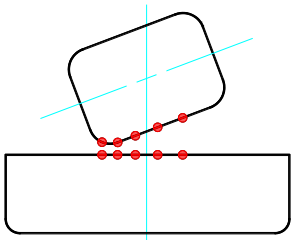

Fig. 15. Inclined rollers contact with the inner ring

Contact analysis is performed for the roller bearing with the best crowning and a misalignment error (tilting angle θ=0.05 degree) under the radial load *P*=50.5kN. The other conditions are the same as Sections 4.3. Figure 16 is the calculated contact pressure distributed on the roller 4 when θ=0.05 degree. By comparing Fig. 16 with Fig. 13(a), it is found that the contact pressure distribution is changed from a uniform distribution into a slope distribution because of the misalignment error. Also, the maximum pressure is changed from 3469MPa into 3597MPa by the misalignment error. Since this change shall reduce the bearing life, it is an important thing not to allow the bearing to have greater misalignment error in a practical use.

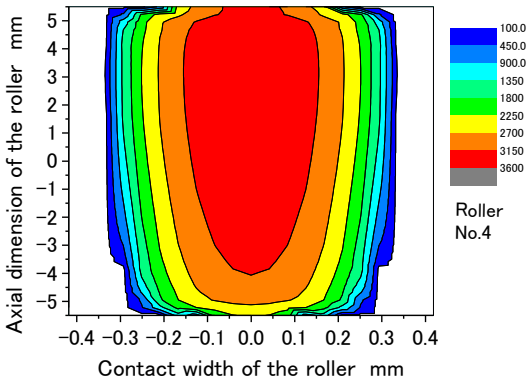

Fig. 16. Contact pressure distribution on the roller 4 (MPa) (with misalignment error)

5. Internal stresses of the roller

Internal stresses are also analyzed for the roller 4 under the conditions of load 50.5kN and best crowning. The stress distributions on Section 1 and Section 2 defined in Fig. 8 are given in Figs. 17 and 18.

Figure 17 (a) is the normal stress σ_y distributed on Section 1. From Fig. 17(a), it is found that a great compressive stress about 4100MPa exists on the roller contact surfaces and the stresses are calculated to be symmetrically distributed vertically, a very reasonable result. It is also found that the edge-loads at the two ends of the roller disappeared very well because of the roller crowning. Figure 17 (b) is the shear stress τ_{yz} distributed on Section 1. From Fig. 17(b), it is found that a great shear stress about 262MPa exists at the two ends of the roller and also the shear stress is symmetrically distributed diagonally. The shear stress at the middle of the contact length is not greater than that at the two ends.

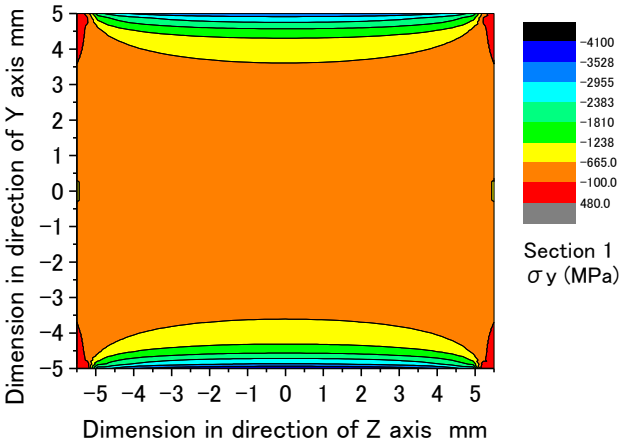

(a) The normal stress σ_y distribution

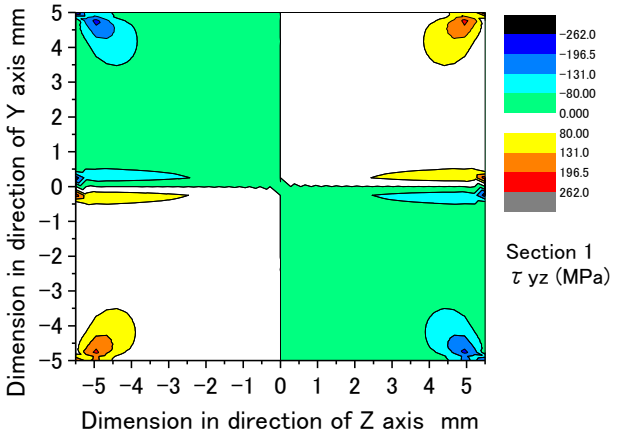

(b) The shear stress τ_{yz} distribution

Fig. 17. The stress distributions on Section 1

Figure 18 (a) is the normal stress σ_y distributed on Section 2. From Fig. 18(a), it is found that a great compressive stress about 4200MPa exists on the contact surface of the roller and the stress is symmetrically distributed vertically. Figure 18 (b) is the shear stress τ_{xy} distributed on Section 2. From Fig. 18(b), it is found that a great shear stress about 1280MPa exists near the contact boundaries of the roller. Also the shear stress is symmetrically distributed diagonally.

Based on the results of Fig. 17(b) and Fig. 18(b), it can be guessed that the roller bearing shall have a fatigue failure at the two ends and near the contact boundaries of the roller, not at the center of the contact area.

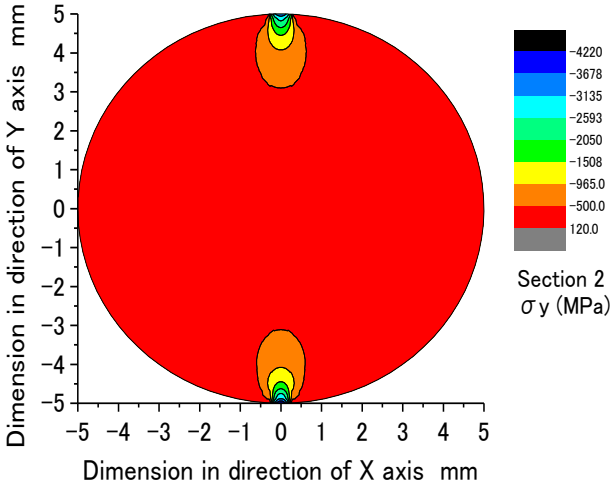

(a) The normal stress σ_y distribution

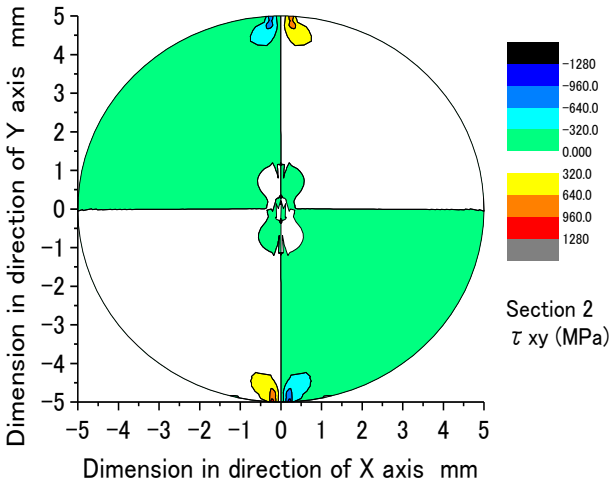

(b) The shear stress τ_{xy} distribution

Fig. 18. The stress distributions on Section 2

6. Conclusions

Contact analysis is conducted successfully for a roller bearing with a crowning and misalignment error using a newly developed numeric method.

The edge-loads are analyzed successfully for the roller bearing when the rollers are not crowned. It is found that the rate of edge-load is about 26% when the rollers are not crowned.

Contact pressures on rollers are also analyzed successfully for the roller bearing when the rollers are crowned using *Johson-Gohar*'s curve. It is found that the maximum contact pressure is reduced about 6% when the rollers are crowned and the quantity of crowning is determined by the basic dynamic load rating. The maximum contact pressure can be further reduced about 11% if the quantity of crowning is determined by the maximum roller load.

The effect of the misalignment error on the contact pressure of the roller is also investigated successfully. It is found that the maximum contact pressure is increased about 3.7% if the bearing has 0.05-degree misalignment error.

Finally, internal stresses of the rollers are analyzed. Position of the maximum shear stress is determined according to the calculation results.

References

[1] C. A. Moyer, Comparing surface failure modes in bearings and gears: appearances vs. mechanisms, Gear Technology, July/August (1992) 34-42.

[2] E. V. Zaretsky, Quest for the 3 million DN Bearing: A history, NTN Technical Review (in Japanese), 67 (1998) 7-19

[3] F. Sadeghi, B. Jalalahmadi, T. S. Slack, N. Raje, N. K. Arakere, A review of rolling contact fatigue, Trans. ASME, J. Trib., 131-1 (2009) 134-139, https://doi.org/10.1115/1.3209132.

[4] K. Stadler, A. Stubenrauch, Premature bearing failures in wind gearboxes and white etching cracks, Power Transmission Engineering, Oct. (2014) 34-40.

[5] S. Miyakawa, Y. Nishimura, S. Nakazawa, N. Shioya, Characterization of white etching area in a ball of deep groove ball bearing, Trans., JSME (in Japanese), 84-868 (2018) 1-12, https://doi.org/10.1299/transjsme.18-00034.

[6] M. R. Lovell, M. M. Khonsari, R. D. Marangoni, Friction analysis of MoS_2 coated ball bearing: A three-dimensional finite element analysis, Trans. ASME, J. Trib., 119 (1997) 754-763.

[7] H. Zhao, Analysis of load distributions within solid and hollow roller bearings, Trans. ASME, J. Trib., 120-1 (1998) 134-139.

[8] S. Kamamoto, K. Fujimoto. and T. Yamamoto, Research on crowning profile to obtain maximum load carrying capacity for roller bearings, KOYO Engineering Journal English Edition 159 (2001) 47-52.

[9] T. L. Krantz, On calculation methods and results for straight cylindrical roller bearing deflection, stiffness and stress, Proceedings of the ASME International Design Engineering Technical Conferences & Computers and Information in Engineering Conference, Washington, DC, (2011) 1-12.

[10] Y. Guo, R. G. Parker, Stiffness matrix calculation of rolling element bearings using a finite element/contact mechanics model, Mech. Mach. Theory 51 (2012) 32-45, https://doi.org/10.1016/j.mechmachtheory.2011.12.006.

[11] R. Tomovic, Calculation of the necessary level of external radial load for inner ring support on q rolling elements in radial bearing with internal radial clearance, Int. J. Mech. Sci., 60 (2012) 23-33, https://doi.org/10.1016/j.ijmecsci.2012.04.002.

[12] H. Wang, S. Dai, Study on contact finite element simulation of the high-angular contact thrust ball bearing, Computer simulation 1 (2013) 1-70.

[13] Z. Qi, G. Wang, Z. Zhang, Contact analysis of deep groove ball bearings in multibody systems, Multibody system dynamics 33 (2) (2015) 115-141.

[14] H. Nagatani, A new resolution to contact problem of roller bearings (in Japanese), The Tribology 6 (346) (2016) 44-46.

[15] C. Bovet, L. Zamponi, An approach for predicting the internal behaviour of ball bearings under high moment load, Mech. Mach. Theory 101 (2016) 1-22, https://doi.org/10.1016/j.mechmachtheory.2016.03.002.

[16] J. Zhang, B. Fang, Y. Zhu, J. Hong, A comparative study and stiffness analysis of angular contact ball bearings under different preload mechanisms, Mech. Mach. Theory 115 (2017) 1-17, https://doi.org/10.1016/j.mechmachtheory.2017.03.012.

[17] C. Machado, M. Guessasma, E. Bellenger, An improved 2D modeling of bearing based on DEM for predicting mechanical stresses in dynamic, Mech. Mach. Theory 113 (2017) 53-66, https://doi.org/10.1016/j.mechmachtheory.2017.01.005.

[18] S. Li, A mathematical model and numeric method for contact analysis of rolling bearings, Mech. and Mach. Theory, 119 (2018) 61-73, https://doi.org/10.1016/j.mechmachtheory.2017.08.020.

[19] P. M. John, R. Gohar, Roller bearings under radial and eccentric loads, Tribology International 14 (1981) 131-136.

[20] Product catalogue of NTN corporation.

[21] G. Lungberg, Elastic contact between two semi-infinite bodies, Forschung auf den Gebiete des Ingenieurwesen (in German), 5 (1939) 201-211.